

Nighttime Thermal Infrared Image Colorization with Feedback-based Object Appearance Learning

Fu-Ya Luo, Shu-Lin Liu, Yi-Jun Cao, Kai-Fu Yang, Chang-Yong Xie, Yong Liu,
and Yong-Jie Li, *Senior Member, IEEE*

Abstract—Stable imaging in adverse environments (e.g., total darkness) makes thermal infrared (TIR) cameras a prevalent option for night scene perception. However, the low contrast and lack of chromaticity of TIR images are detrimental to human interpretation and subsequent deployment of RGB-based vision algorithms. Therefore, it makes sense to colorize the nighttime TIR images by translating them into the corresponding daytime color images (NTIR2DC). Despite the impressive progress made in the NTIR2DC task, how to improve the translation performance of small object classes is under-explored. To address this problem, we propose a generative adversarial network incorporating feedback-based object appearance learning (FoalGAN). Specifically, an occlusion-aware mixup module and corresponding appearance consistency loss are proposed to reduce the context dependence of object translation. As a representative example of small objects in nighttime street scenes, we illustrate how to enhance the realism of traffic light by designing a traffic light appearance loss. To further improve the appearance learning of small objects, we devise a dual feedback learning strategy to selectively adjust the learning frequency of different samples. In addition, we provide pixel-level annotation for a subset of the Brno dataset, which can facilitate the research of NTIR image understanding under multiple weather conditions. Extensive experiments illustrate that the proposed FoalGAN is not only effective for appearance learning of small objects, but also outperforms other image translation methods in terms of semantic preservation and edge consistency for the NTIR2DC task.

Index Terms—Thermal infrared image colorization, image-to-image translation, generative adversarial networks, feedback-based learning, nighttime scene perception.

I. INTRODUCTION

NIGHTTIME scene perception is a fundamental yet challenging computer vision tasks. Despite its superiority in texture capture, visible spectrum-based perception systems fail in total darkness conditions and do not enable accurate imaging of dazzling areas. On the contrary, the insensitivity to lighting conditions and strong penetration in hazy environments make thermal infrared-based imaging one of the promising solutions for nighttime scene perception [1], [2]. However, the low contrast and monochromatic nature of thermal infrared (TIR) images hinder human interpretation [3]

and subsequent deployment of RGB-based models. Therefore, the translation from nighttime TIR images into corresponding daytime color (DC) images (abbreviated as NTIR2DC) is of great significance, which not only benefits the rapid understanding of nighttime scenes, but also reduces the annotation cost of NTIR image analysis tasks through existing visible-based datasets and algorithms.

Due to the difficulty of acquiring a large number of pixel-level aligned cross-domain image pairs, more efforts [4], [5] have been devoted to the implementation of NTIR2DC tasks using unsupervised image-to-image (I2I) translation methods. Unsupervised I2I translation aims to learn mappings between different image domains under the condition of unpaired samples [6]. In recent years, driven by the promising advances in image generation, generative adversarial networks (GANs) [7] have attracted extensive attention in the field of unsupervised I2I translation. For example, Zhu *et al.* [8] proposed CycleGAN to encourage cycle-consistency between the reconstructed image after inverse translation and the original image. To enhance the diversity of translation results, [9] and [10] learned separated image content representations and style representations. ToDayGAN [11] utilized multiple discriminators to improve night-to-day translation performance. PearlGAN [4] introduced a top-down guided attention module and corresponding losses to reduce semantic encoding entanglement in the NTIR2DC task.

Despite the impressive results achieved by previous approaches, the problem of how to mitigate the context dependence of object translation is under addressed. Moreover, it is under-explored how to improve the colorization performance of small object categories (SOC) without semantic annotation. As shown in Fig. 1, previous methods consistently failed to generate plausible traffic lights. To handle these limitations mentioned above, a GAN network incorporating Feedback-based Object Appearance Learning, referred to as FoalGAN, is proposed in this paper.

In the NTIR2DC task, we observed that there may be large differences in the translation results of same objects under different contextual conditions, which is defined by us as the context dependence of object translation. Inspired by Mixup [12] in the enhancement of model generalization, we devise an occlusion-aware mixup (OAMix) module to fuse fake objects with real images, constraining the consistency of object translation through an appearance consistency loss to reduce context dependence. Unlike previous approaches, the proposed OAMix utilizes pseudo-labels to avoid the occlusion of cross-domain objects, and an adaptive luminance adjustment strategy

Fu-Ya Luo, Yi-Jun Cao, Kai-Fu Yang and Yong-Jie Li are with the MOE Key Laboratory for Neuroinformation, the School of Life Science and Technology, University of Electronic Science and Technology of China, Chengdu 610054, China. E-mail: luofuya1993@gmail.com, yijuncaoo@gmail.com, yangkf@uestc.edu.cn, lij@uestc.edu.cn.

Shu-Lin Liu, Chang-Yong Xie and Yong Liu are with the Naval medical center of PLA, Shanghai, 200433, China. E-mail: shulinliu@smmu.edu.cn, xiechangyong@smmu.edu.cn, mike_ly@163.com. (*Corresponding author: Shu-Lin Liu, Yong Liu.*)

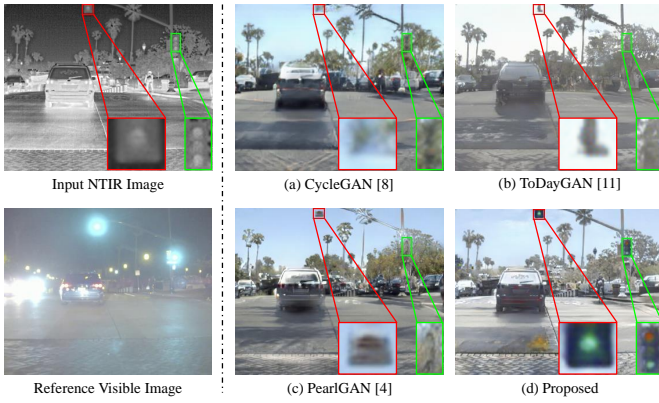


Fig. 1. Visual comparison of colorization results. The areas in the red and green boxes deserve attention.

is designed to enhance the naturalness of the synthesized NTIR images.

For small object translation, lack of supervision and low percentage contributed to the loss of objective function make feature learning of SOC difficult, and the random sample learning strategy of GAN networks worsens this issue. Compared with artificial neural networks, humans have powerful learning capabilities that allow them to master a wide range of skills, and feedback during learning process can help learners improve the systematicity of their strategies to better acquire and apply knowledge [13], [14]. Motivated by this feedback-based learning scheme, we propose a dual feedback learning strategy to improve the translation performance of SOC. Specifically, the appearance consistency loss of the current iteration modulates the input sample selection for the next iteration through a feedback connection, which adaptively adjusts the learning frequency of small object samples in both domains.

In addition, to illustrate how to facilitate the translation of small objects with the proposed framework, we select the traffic light as a representative example in nighttime street scenes to show how to enhance the colorization performance of such object by designing an elaborate traffic light appearance loss. Furthermore, regarding the evaluation of NTIR2DC methods, previous methods have been studied almost exclusively on NTIR datasets under cloudy conditions, what if the images are collected under rainy conditions? And what if the training set images contain multiple types of weather? To explore these concerns, we conduct further experiments on the Brno [15] dataset containing NTIR images of multiple weather conditions. Further, we sample a subset for pixel-level semantic annotation. Exhaustive experiments show that the proposed method not only improves the colorization performance of SOC, but also significantly outperforms existing translation methods in terms of semantic and edge preservation. The main contributions of this study are:

- An OAMix module and the corresponding appearance consistency loss are designed to reduce the context dependence of object translation and enhance the generalization capacity of model.
- A dual feedback learning strategy is proposed to adap-

tively adjust the learning frequency of small object samples, which is beneficial to improve the translation performance of small objects.

- A traffic light appearance loss considering both luminance and color is proposed to enhance the overall realism of the traffic light, which may provide inspiration to enhance specific small objects under specific conditions for specific tasks.
- We annotate a subset of the Brno dataset with semantic masks, which may catalyze the researches of NTIR image understanding for multiple weather conditions.
- The experimental results of the NTIR2DC task demonstrate the superiority of the proposed FoalGAN¹ in terms of small-object colorization and semantic consistency of translation.

The rest of this paper is organized as follows. Section II summarizes related work about TIR image colorization and I2I translation. Section III introduces the architecture of the proposed FoalGAN. Section IV presents the experiments on the FLIR and Brno datasets. Section V draws the conclusions.

II. RELATED WORK

In this section, we briefly review previous work on TIR image colorization, unpaired I2I translation, neural networks with feedback connections, and mask-based mixup strategy.

A. TIR Image Colorization

TIR image colorization aims to map a grayscale TIR image to a three-channel RGB image without changing semantics. Based on the demand for paired RGB images, TIR image colorization methods can be divided into two categories: supervised and unsupervised. The supervised approach forces the model to maximize the similarity of its output to the aligned RGB image. For example, Berg *et al.* [16] realized TIR image colorization by introducing separate luminance and chrominance loss. In order to increase the naturalness of the results, more efforts [17]–[19] have focused on combining pixel-level content loss with adversarial loss to optimize the mapping from TIR to RGB images. SCGAN [20] jointly predicted the colorization and saliency map to reduce semantic confusion and color bleeding. Compared with supervised methods, unsupervised methods do not require finely aligned cross-domain samples, which greatly reduces data collection costs and extends their applicability. Most unsupervised colorization methods utilize the GAN model to implement the image translation from TIR to visible spectrum. For example, Nyberg *et al.* [21] exploited the CycleGAN [8] model to achieve unsupervised TIR image colorization. PearlGAN [4] was proposed to reduce semantic encoding entanglement and edge distortion in the NTIR2DC task. DlamGAN [5] introduced a dynamic label mining module and a segmentation loss to encourage the semantic consistency of NTIR colorization process. To enhance the semantic preservation of small sample categories, MornGAN [22] introduced a memory-guided collaborative

¹The source code will be available at <https://github.com/FuyaLuo/FoalGAN/>.

attention strategy. Despite their encouraging progress, few efforts have been made to improve the colorization performance of SOC.

B. Unpaired I2I Translation

The purpose of unpaired I2I translation is to learn a transformation function through unpaired samples to achieve cross-domain mapping of images. Zhu *et al.* [8] made the earliest effort to get rid of the requirement of aligned image pairs by using cycle consistency loss, leading to the recent surge of interest in methods for unpaired I2I translation. On the basis of CycleGAN, UNIT [23] replaced the domain-specific latent space with a shared latent space. Recent works further boosted the generation performance of night-to-day image translation by introducing multiple discriminators [11], additional decoders [24], or auxiliary detection branches [25], [26]. In order to reduce content distortion during translation, semantic consistency loss is more often introduced into GAN models [27], [28]. Considering the demand for incremental learning in practical applications, Tan *et al.* [29] proposed an IncrementalGAN that can incrementally learn new domains without requiring the training data from the previously learned domains. Although these approaches have obtained impressive results, how to improve the translation performance of SOC under unlabeled conditions remains under-explored. In addition, the issue of how to reduce the context dependence of object translation has been little studied.

C. Neural Networks with Feedback Connections

Feedback is defined as an event that reroutes the (partial or full) output of a system back into the input and as part of an iterative cause-and-effect process [30]. Feedback connections are beneficial for humans to achieve flexible pattern recognition in complex and rapidly changing environments [31]–[33]. Inspired by this, many researchers [34], [35] have introduced feedback connections in the design of deep networks. For example, DasNet [34] utilized a feedback structure to dynamically adjust the sensitivity of each convolutional filter during classification. To achieve iterative inference, some studies [35], [36] employed a convolutional recurrent neural network model to pass the output of each iteration through a hidden state to the next iteration. Song *et al.* [37] incorporated a feedback mechanism into the model to reuse the intermediate results of each stream to achieve single image dehazing. Unlike previous approaches that focus on feature integration, the proposed feedback connection in this work collaboratively adjusts the selection of input samples for both domains based on the learning state of model, which does not increase the computational and time costs of model inference.

D. Mask-based Mixup Strategy

Mixup is a data augmentation strategy that combines sample pairs and their labels in a linear fashion [12]. Driven by its success in improving model generalization, the mask-based mixup strategy has been widely adopted for various computer vision tasks [38]–[40]. For example, CutMix [38] cut and

past a rectangular box area from one image to another. In the unlabeled condition, ClassMix [39] cut and pasted half of the classes of one image to another image based on the predicted masks. RICAP [41] stitched four images into one image after cropping out small pieces at a certain ratio. Considering the cross-domain context dependency, CAMix [40] first used the spatial distribution of the source domain and the contextual relationship of the target domain to estimate the contextual mask, and then performed subsequent domain mixup based on the mask. Despite the remarkable progress of the mask-based mixup strategy, how to avoid the unrealistic problem (e.g., a bus appears in the abdomen of a pedestrian) caused by object occlusion in fused images under unlabeled conditions remains to be explored. In addition, how to reduce the luminance differences between patches of TIR image mixup is under-resolved.

III. PROPOSED METHOD

In this section, we first present the overview of the proposed FoalGAN. Subsequently, we briefly explain our baseline model. Then, the details of bias correction in the fake NTIR image branch are described. Next, we explicate the OAMix module. Afterward, the traffic light appearance loss enhancing the appearance realism of traffic lights is explained. Then, the dual feedback learning strategy is specified. Finally, we illustrate the total loss of FoalGAN.

A. Model's Overview and Problem Formulation

The overall framework is shown in Fig. 2. We first choose MornGAN [22] as baseline model to encourage semantic consistency of translation, and its total loss is abbreviated as \mathcal{L}_{base} . Then, we introduce a bias correction loss \mathcal{L}_{bc} to reduce the bias of the fake NTIR image branch. Next, we devise an OAMix module and an appearance consistency loss \mathcal{L}_{ac} to moderate the context dependence of SOC translation. Subsequently, a traffic light appearance loss \mathcal{L}_{tla} is designed to enhance the realism of traffic lights in colorization results. Finally, we propose a dual feedback learning strategy to rationally allocate the learning frequency of samples containing SOC, which aims to improve the translation performance of SOC while reducing the degradation of learning for other categories.

In the rest of the paper, domain A and domain B denote the DC image set and NTIR image set, respectively, abbreviated as X^A and X^B . Taking the translation from domain A to domain B as an example, we denote the input image pair of domain A and B as $\{x_{ra}, x_{rb}\}$, the generator G_{AB} contains an encoder of domain A and a decoder of domain B, and the discriminator D_B aims to distinguish the real image x_{rb} from the translated image x_{fb} (i.e., $G_{AB}(x_{ra})$). Similarly, the inverse mapping includes generator G_{BA} and discriminator D_A .

B. Baseline Model

MornGAN [22] is proposed to improve the colorization performance of small sample categories in the NTIR2DC task. Specifically, two semantic segmentation networks (i.e., S_A and

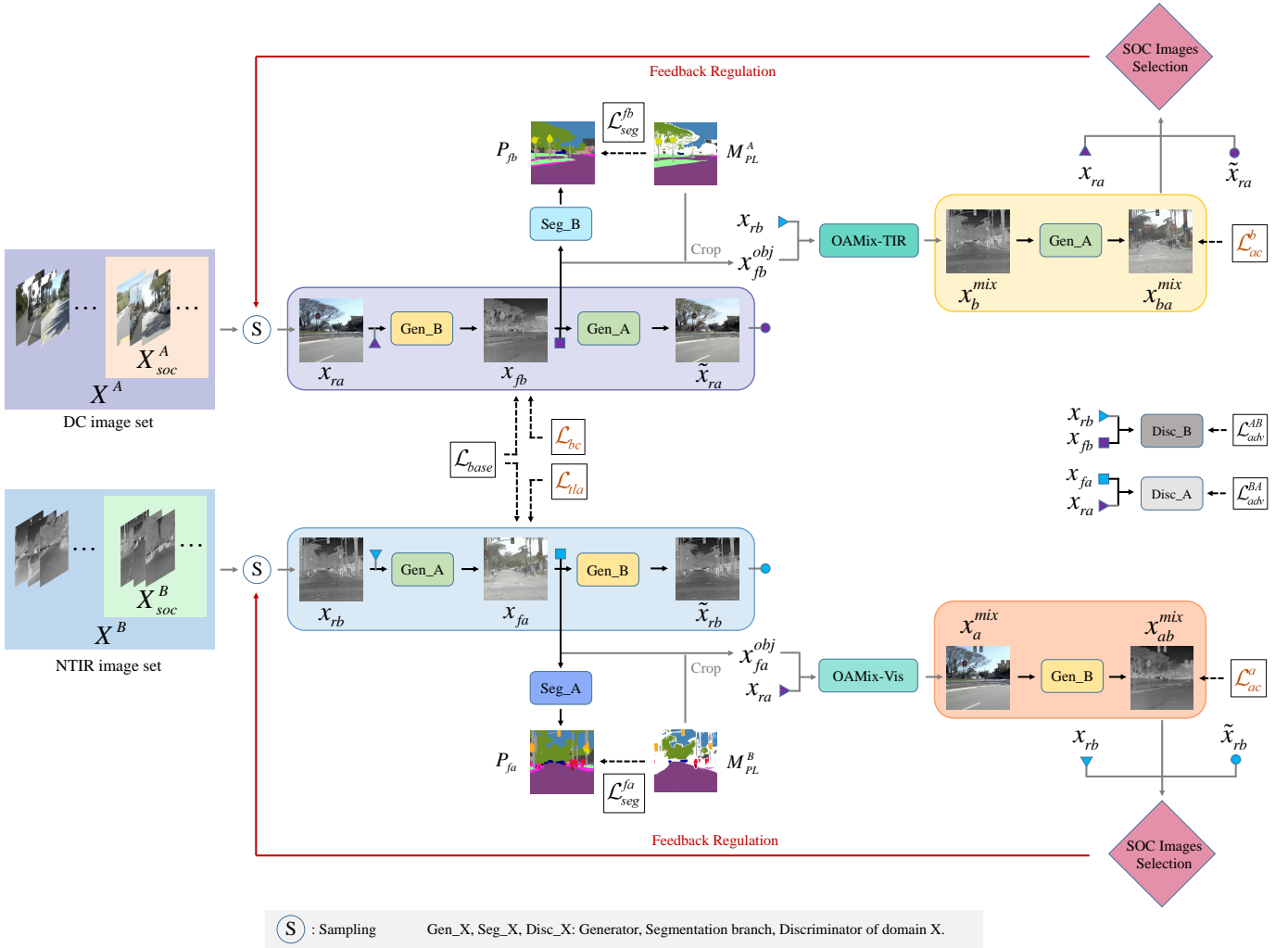


Fig. 2. The overall architecture of the proposed method. x_{ra} and x_{rb} are one image in the DC and NTIR domains, respectively, whose sampling is modulated by the feedback from the SOC image selection module of the previous iteration. The translation results of the input image pairs, denoted as x_{fb} and x_{fa} , are first mixed with the real images (i.e., x_{rb} and x_{ra}) through the OAMix module under the guidance of pseudo-labels (i.e., M_{PL}^A and M_{PL}^B). The corresponding appearance consistency loss (i.e., \mathcal{L}_{ac}^a and \mathcal{L}_{ac}^b) then encourages the robustness of the SOC translation against background variations. And the samples containing SOC in the DC and NTIR domains are denoted as X_{soc}^A and X_{soc}^B , respectively.

S_B) and segmentation losses (i.e., \mathcal{L}_{seg}^{fa} and \mathcal{L}_{seg}^{fb}) are introduced to encourage the semantic consistency of translation. Due to the lack of semantic annotation, two existing segmentation models (i.e., Detectron2 [42] and HMSANet [43]) are first used to predict the pseudo-labels (M_{PL}^A) of DC images. The pseudo-labels (M_{PL}^B) of NTIR images are then obtained by an online semantic distillation module, which is subsequently stored in a memory unit. When the stored quantity meets the condition, the memory-guided sample selection strategy is triggered, and then similar NTIR images are recalled for the input DC images for collaborative learning. Finally, adaptive collaborative attention loss is used to encourage the inter-domain similarity of features of small sample categories. In addition, the conditional gradient repair loss is introduced to reduce edge degradation during translation, and a scale robustness loss is used to improve the insensitivity of the model to the object scale.

C. Bias Correction in the Fake NTIR Image Branch

Although MornGAN can effectively improve the colorization performance of small sample categories, how to reduce the various types of biases in the fake NTIR image branch during training is under-resolved. As shown in Fig. 3, the biases in the fake NTIR branch are divided into three main types: mapping bias of semantic segmentation, artifact bias of image translation and color bias of image reconstruction. Since the two branches in the model are highly coupled, the presence of these biases is detrimental to the appearance learning of SOC in both domains. In this section, we focus on how to correct for these biases.

1) *Mapping Correction for Semantic Segmentation*: Due to the lack of semantic annotation and the existence of some artifacts in the fake NTIR images, some mapping bias occurs in the semantic learning of fake NTIR images. Among them, there are two mapping biases that are highly relevant to the semantic prediction of SOC. The first bias is mapping the high

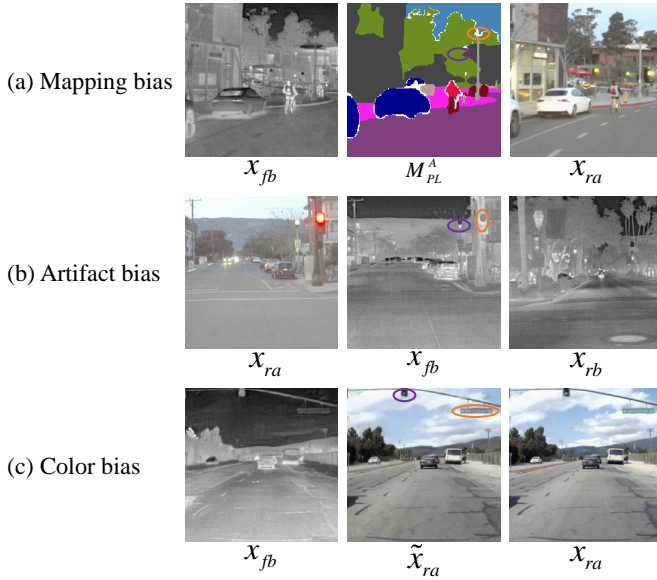


Fig. 3. Example images of biases in the fake NTIR image branch. The orange and purple boxes are two examples of the corresponding bias. x_{ra} , x_{rb} , x_{fb} , \tilde{x}_{ra} , and M_{PL}^A denote the real DC image, the real NTIR image, the fake NTIR image, the reconstructed DC image, and the pseudo-labels of domain A, respectively.

luminance regions of the fake NTIR images to the vegetation category, and the second is mapping the streetlight regions to other categories, as shown in Fig. 3(a).

In order to reduce the first mapping bias, we set the semantic labels corresponding to regions with high luminance (i.e., greater than the luminance mean) in the vegetation category in the fake NTIR images to “uncertain” (i.e., no loss calculation). For the second bias, we first add streetlight to the definition of the category set. Then, the masks of SOC for DC images are predicted by the HMSANet [43] trained on the Mapillary [44] dataset, which is subsequently used to update the pseudo-labels M_{PL}^A .

2) *Artifact Correction for Image Translation*: Compared with supervised I2I translation, unpaired I2I translation usually produces local artifacts due to the lack of pixel-level labels. In general, the temperature of the luminous areas in street and traffic lights is usually higher than that of the neighboring regions under nighttime conditions. However, when no specific strategy is taken into account, bright areas in DC images belonging to streetlights and traffic lights become darker after translation, which deviates from the temperature distribution in the nighttime scenes, as shown in Fig. 3(b). Therefore, we propose an artifact bias correction loss \mathcal{L}_{abc} to reduce such limitation. In order to correct the luminance bias of street lights, we propose a street light luminance adjustment loss \mathcal{L}_{sla} . We have observed that the temperature of luminous street light is usually higher than that of vegetation, e.g., the trees along the street. Motivated by this observation, the loss \mathcal{L}_{sla} aims to encourage that the minimum value of the bright areas of streetlight in the fake NTIR image should be greater than the mean value of vegetation. Specifically, given the minimum value of the bright areas of the streetlight category in the fake NTIR image, denoted as \tilde{t}_{fb}^{sl} , and the mean value of the

vegetation category, denoted as \bar{t}_{fb}^{veg} , the loss \mathcal{L}_{sla} is defined as

$$\mathcal{L}_{sla} = \max \left(\bar{t}_{fb}^{veg} - \tilde{t}_{fb}^{sl} + \theta_{tem}, 0 \right), \quad (1)$$

where θ_{tem} is a threshold value to control the temperature difference between classes.

Due to the spatial hierarchy of the luminance distribution of traffic lights, a simple minimum constraint to reduce the artifact bias of traffic lights is sub-optimal. Therefore, inspired by the observation that the temperature of luminous region is higher compared with that of other regions, we propose another traffic light luminance adjustment loss \mathcal{L}_{tla} to encourage the consistency of the luminance distribution during translation. Specifically, given a grayscale map of DC image as $I_{ra}^g \in \mathbb{R}^{H \times W}$, we first subtract the mean of traffic light region, then perform dot product using the binary mask of traffic light, and finally perform vectorization to obtain the result noted as $V_{ra}^{tl} \in \mathbb{R}^{1 \times N}$. And N denotes the product of H and W . Similarly, the corresponding result of the fake NTIR image is denoted as $V_{fb}^{tl} \in \mathbb{R}^{1 \times N}$. Then, the loss \mathcal{L}_{tla} can be calculated based on cosine similarity as

$$\mathcal{L}_{tla} = \max \left(\theta_{sim} - \frac{V_{ra}^{tl} \cdot V_{fb}^{tl}}{\|V_{ra}^{tl}\|_2 \cdot \|V_{fb}^{tl}\|_2}, 0 \right), \quad (2)$$

where θ_{sim} denotes the similarity threshold and $\|\cdot\|_2$ denotes the L2 norm.

Since the region corresponding to the SOC in the pseudo-labels is noisy, the introduction of the above mask-based loss can lead to degradation of edge consistency. Considering that structured gradient alignment (SGA) loss [4] can encourage the edge consistency of translation, we regularize the geometric consistency of corresponding region using SGA loss \mathcal{L}_{sga} . Concretely, the edge map of the DC image and the gradient map of the fake NTIR image after masking the street light and traffic light are denoted as EM_{ra}^l and GM_{fb}^l , respectively. Then, the artifact bias correction loss can be written as

$$\mathcal{L}_{abc} = \mathcal{L}_{sla} + \mathcal{L}_{tla} + \lambda_{sga} \mathcal{L}_{sga} (GM_{fb}^l, EM_{ra}^l), \quad (3)$$

where λ_{sga} denotes the weight of SGA loss, which is set to 0.5 according to [4].

3) *Color Correction for Image Reconstruction*: Although PearlGAN [4] can effectively reduce the reconstruction error of images by combining the smooth L1 loss [8] \mathcal{L}_{sl1} and SSIM [45] loss \mathcal{L}_{ssim} , the reconstruction of SOC regions will often show color distortion due to the small percentage of contribution to the total loss, as shown in Fig. 3(c). To address this issue, with reference to [4], we first define a mask-based image distance function $MIDF(\cdot)$. Given the original image $I_{ori} \in \mathbb{R}^{C \times H \times W}$, the reconstructed image $I_{rec} \in \mathbb{R}^{C \times H \times W}$, and the binary mask $M_b \in \mathbb{R}^{H \times W}$, the image distance corresponding to the mask region can then be expressed as

$$\begin{aligned} MIDF(M_b, I_{rec}, I_{ori}) = & \mathcal{L}_{ssim}(M_b \odot I_{rec}, M_b \odot I_{ori}) + \\ & \lambda_{sl1} \mathcal{L}_{sl1}(M_b \odot I_{rec}, M_b \odot I_{ori}), \end{aligned} \quad (4)$$

where \odot denotes element-wise multiplication with channel-wise broadcasting, and the weight λ_{sl1} is set to 10.0 according to [8].

Then, we propose a color bias correction loss \mathcal{L}_{cbc} based on the function $MIDF(\cdot)$ to reduce the color distortion involved in reconstruction process. In particular, given the binary mask M_{SOC}^A of SOC, the reconstructed image \tilde{x}_{ra} , and the original image x_{ra} , the loss \mathcal{L}_{cbc} can then be formulated as

$$\mathcal{L}_{cbc} = MIDF(M_{SOC}^A, \tilde{x}_{ra}, x_{ra}). \quad (5)$$

Finally, the total bias correction loss \mathcal{L}_{bc} is the sum of \mathcal{L}_{abc} and \mathcal{L}_{cbc} . With the introduction of bias correction loss, the SOC reconstruction error of fake NTIR branch will be significantly reduced, which paves the way for improving the colorization performance of the SOC in real NTIR images.

D. OAMix Module

To generalize the mapping of the SOC in fake NTIR branch to real NTIR, we propose an OAMix module and an appearance consistency loss. For the mixing of NTIR images, the preservation of the contours of objects is crucial for the recognition of objects due to lack of color and texture information. Moreover, occlusion between objects may cause unreasonable mixing of DC images, e.g., a motorcycle appears in the face of pedestrians. Therefore, unlike previous methods, we propose an OAMix module to avoid object occlusion during image mixing. In addition, considering the sparsity of SOC samples, the mixed SOC objects contain instances from both the original image and its horizontally flipped image, an example image is shown in Fig. 4.

Taking the DC domain as an example, given the fake DC image $x_{fa} \in \mathbb{R}^{C \times H \times W}$ and the real DC image $x_{ra} \in \mathbb{R}^{C \times H \times W}$, and their semantic pseudo-labels $M_{PL}^B \in \mathbb{R}^{H \times W}$ and $P_{ra} \in \mathbb{R}^{H \times W}$, the OAMix module aims to fuse the SOC in x_{fa} with x_{ra} . Specifically, we first obtain the binary masks of objects and roads of x_{ra} by P_{ra} , denoted as M_{obj}^A and M_{road}^A , respectively. Then, given the SOC set \mathcal{C}_{so} , for the category $c_i \in \mathcal{C}_{so}$, we can obtain the binary mask $M_i^B \in \{0, 1\}^{H \times W}$ for the category c_i of x_{fa} . Subsequently, we can obtain all the connected regions of M_i^B based on the connectivity. For the j_{th} connected region $M_{i,j}^B$ whose area is larger than the threshold, if the intersection of $M_{i,j}^B$ and M_{obj}^A is empty, we determine whether it is a subset of the original mixing mask $Q^{Ao} \in \{0, 1\}^{H \times W}$ according to the following rules

$$Q_{i,j}^{Ao} = \begin{cases} M_{i,j}^B, & \text{if } c_i \notin \mathcal{C}_{veh}. \\ M_{i,j}^B, & \text{if } c_i \in \mathcal{C}_{veh}, M_{i,j}^B \cap M_{road}^A \neq \emptyset. \\ 0, & \text{otherwise.} \end{cases} \quad (6)$$

\mathcal{C}_{veh} denotes the set of categories that belong to vehicle. Given that the number of \mathcal{C}_{so} is N_{soc} , and the number of connected regions corresponding to the i_{th} category is N_{cr}^i , we can obtain the original mixing mask by

$$Q^{Ao} = \sum_{i=1}^{N_{soc}} \sum_{j=1}^{N_{cr}^i} Q_{i,j}^{Ao}. \quad (7)$$

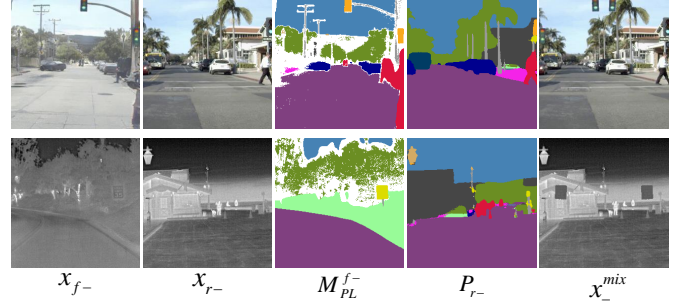


Fig. 4. Example images of the fusion results in two domains obtained by the OAMix module. The first two columns are the input fake and real images, respectively. And the last three columns are the pseudo-labels of the fake images, the predicted masks of the real images and the fusion results, respectively.

Similarly, for the result of horizontal flip of x_{fa} , denoted as x_{fa}^f , we can obtain the corresponding mixing mask Q^{Af} . Next, we can utilize Q^{Ao} and Q^{Af} to obtain the mixed object areas

$$x_{fa}^{obj} = Q^{Ao} \odot x_{fa} + (Q^{Af} - (Q^{Af} \cap Q^{Ao})) \odot x_{fa}^f. \quad (8)$$

And the final mixed image can be represented as

$$x_a^{mix} = x_{fa}^{obj} + (\mathbf{1} - (Q^{Ao} \cup Q^{Af})) \odot x_{ra}. \quad (9)$$

where $\mathbf{1}$ is a binary mask filled with ones. Next, we can use the image distance function $MIDF(\cdot)$ of Eq. (4) to encourage the appearance consistency of SOC objects. Let the translated result of image x_a^{mix} be denoted as x_{ab}^{mix} , then the appearance consistency loss of domain A can be expressed as

$$\mathcal{L}_{ac}^a = MIDF(Q^{Ao}, x_{ab}^{mix}, x_{ra}). \quad (10)$$

Similarly, we can obtain two mixing mask of domain B, denoted as Q^{Bo} and Q^{Bf} , and the mixed object region, denoted as x_{fb}^{obj} . However, due to the temperature difference among NTIR images, direct mixing of x_{fb}^{obj} and x_{rb} may produce obvious stitching edges, which deviate from the temperature distribution of the current scene. Therefore, we propose an adaptive luminance adjustment (ALA) strategy to make the mixing of NTIR images more natural. Considering the high frequency of road areas in traffic images and their relatively uniform temperature distribution, the ALA strategy aims to encourage the average temperature of x_{fb}^{obj} to be similar to that of x_{rb} in road areas. Specifically, let the mean value of x_{fb}^{obj} be μ_{fb}^{obj} and the mean value of the road region of x_{rb} be μ_{rb}^{road} , then the mixed image of domain B can be represented as

$$x_b^{mix} = \frac{\mu_{rb}^{road}}{\mu_{fb}^{obj}} \times x_{fb}^{obj} + (\mathbf{1} - (Q^{Bo} \cup Q^{Bf})) \odot x_{rb}, \quad (11)$$

where the fractional in the first term represents the luminance adjustment factor. When the value of the fractional is greater than 1.0, the mixed object area x_{fb}^{obj} needs to be brightened to adapt to the current scene, and vice versa. Such an adaptive sample fusion not only makes the temperature distribution of the mixed NTIR images more reasonable, but also reduces the overfitting probability of SOC translation.

For the appearance consistency loss of domain B, we introduce conditional gradient repair loss [22] \mathcal{L}_{cgr} to reduce the image gradient disappearance during translation, in addition to the supervised loss on object regions. Specifically, let the translated result of the image x_b^{mix} be denoted as x_{ba}^{mix} , then the appearance consistency loss of domain B can be expressed as

$$\mathcal{L}_{ac}^b = \text{MIDF}(Q^{Bo}, x_{ba}^{mix}, x_{ra}) + \mathcal{L}_{cgr}(Q_{con}^B \odot x_{ba}^{mix}, Q_{con}^B \odot x_{rb}), \quad (12)$$

where Q_{con}^B denotes the binary mask of the context in domain B, which can be represented as

$$Q_{con}^B = \mathbf{1} - (Q^{Bo} \cup Q^{Bf}). \quad (13)$$

Ultimately, the total appearance consistency loss \mathcal{L}_{ac} is the sum of \mathcal{L}_{ac}^a and \mathcal{L}_{ac}^b .

With the introduction of the OAMix module and appearance consistency loss, SOC objects are required to maintain robust translation while the context changes, which helps reduce the context dependence of object translation.

E. Traffic Light Appearance Loss

Although the problem of context dependence has been moderated as above, how to improve the appearance realism of traffic lights in colorization results is under-explored. Under nighttime conditions, traffic lights are very common and the glare from them may largely interface with the depth estimation of their neighboring areas. Hence, reasonable traffic light colorization by the NTIR2DC method is beneficial for fine-grained scene perception. Therefore, considering the luminance and color, a traffic light appearance loss is proposed to enhance the colorization performance of traffic lights.

1) *Traffic Light Luminance Loss*: Previous NTIR2DC methods [4], [22] usually change the luminance distribution of traffic lights during the translation process, i.e., translate the bright regions in the NTIR image into dark regions. This distribution flipping phenomenon deviates from the prevalent mapping relationship between temperature and luminance, i.e., the temperature of the bright regions of traffic lights is higher than that of their neighbors. Therefore, the traffic light luminance loss \mathcal{L}_{tll} is proposed to encourage a positive scale mapping of temperature to luminance.

Specifically, based on the mean luminance of traffic lights in the NTIR image x_{rb} , we can obtain two binary masks M_{tl}^{br} and M_{tl}^{dr} for the traffic light regions, indicating the bright and dark regions of traffic lights, respectively. Then, we can obtain the lowest luminance δ_{tl}^{br} corresponding to M_{tl}^{br} and the average luminance μ_{tl}^{dr} corresponding to M_{tl}^{dr} of the fake DC image x_{fa} . Next, the loss \mathcal{L}_{tll} encourages that the minimum value of the translated high-temperature region should be no less than the mean value of the low-temperature region, which can be formulated as

$$\mathcal{L}_{tll} = \frac{\max(\mu_{tl}^{dr} - \delta_{tl}^{br}, 0)}{\delta_{tl}^{br}}, \quad (14)$$

where the denominator is used for adaptive scaling of the results.

2) *Traffic Light Color Loss and Color Conversion Module*: Although the colors of traffic lights are not unique, they are closely related to spatial locations, i.e., lights that are lit at similar locations usually show same colors. Therefore, the traffic light color loss \mathcal{L}_{tlc} aims to guide the model to learn the correspondence between the colors and the luminous positions. Among the colors of traffic lights, yellow is difficult to be captured by visible cameras due to the short luminous time. Thus, the traffic light colors to be recovered in this paper are mainly red and green. However, due to the chance of data collection, the data of red and green lights are usually unbalanced, which introduces a large bias in color learning. In view of this, we creatively propose a color conversion module to realize the interconversion of red and green.

Given a traffic light instance in a DC image (RGB format), if its aspect ratio is greater than the given threshold, we first flip it vertically and then convert it to HSV format. Next, we obtain the binary masks corresponding to the red and green regions, denoted as M_{rr}^{ins} and M_{gr}^{ins} , respectively, based on the hue values. If M_{rr}^{ins} is greater than M_{gr}^{ins} , we map the red regions to the green regions according to the mapping relationship of hue values. Conversely, the green region is mapped to the red region. Ultimately, the mapped HSV format is then converted to RGB format. The above processing is integrated into the color conversion module. To reduce the learning bias of colors, the random vertical flip of traffic light instances is embedded in the OAMix-TIR module, and its corresponding label x_{ra} is processed using the color conversion module.

Combined with the color conversion module, the loss \mathcal{L}_{tlc} can guide the model to learn the colors of traffic lights more efficiently. Specifically, given the traffic light mask $M_{tl}^B \in \{0, 1\}^{H \times W}$ of the NTIR image, we first divide it into two binary sub-masks—upper and lower, denoted M_{upr}^B and M_{lowr}^B , according to the center height of each instance. Similarly, the two sub-masks of the DC image $x_{ra} \in \mathbb{R}^{C \times H \times W}$ are denoted as M_{upr}^A and M_{lowr}^A , respectively. Then, we use the color conversion module to obtain the bright region mask of each instance, which are subsequently fused to obtain the bright region mask of x_{ra} , denoted as M_{br}^A . For the NTIR image x_{rb} , the corresponding bright region mask of traffic light is the same as M_{tl}^{br} mentioned in the previous subsection, denoted as M_{br}^B . Next, for the traffic light region of x_{ra} , the average color feature of the bright region (e.g., red light) in its upper sub-masks, denoted as $F_{ub}^{ra} \in \mathbb{R}^{C \times 1 \times 1}$, can be expressed as

$$F_{ub}^{ra} = \frac{H \times W}{N_{ub}^A} \times \mathcal{GAP}(M_{upr}^A \odot M_{br}^A \odot x_{ra}), \quad (15)$$

where N_{ub}^A denotes the sum of the binary masks $M_{upr}^A \odot M_{br}^A$, and $\mathcal{GAP}(\cdot)$ denotes the global average pooling operation. Similarly, we can obtain the average color feature F_{lb}^{ra} for the bright region (e.g., green light) in the lower sub-masks, and the upper and lower features corresponding to the fake DC image x_{fa} , denoted as F_{ub}^{fa} and F_{lb}^{fa} , respectively. Then, the color distance of the upper sub-masks can be presented as

$$d_{uu}^{fr} = \sqrt{\sum_{k=1}^C \left((F_{ub}^{fa} - F_{ub}^{ra})^2 \right)_k}. \quad (16)$$

Similarly, we can obtain the color distance d_{ll}^{fr} for the lower half. Due to the small difference between red and green in the root mean square distance and the sparsity of green lights on traffic images, an appropriate weight on d_{ll}^{fr} is necessary for the learning of green lights. To encourage that the intra-class distance (i.e., d_{ll}^{fr}) of colors should be smaller than the inter-class distance (i.e., the distance between F_{lb}^{fa} and F_{ub}^{ra} , denoted as d_{lu}^{fr}), we set the weighting factor as

$$\beta_w = \frac{1}{\min(d_{ll}^{fr}, d_{lu}^{fr}) + \tau}, \quad (17)$$

where τ is a constant to prevent the denominator from being zero as well as to control the range of values, which is empirically set to 0.05. Ultimately, the complete color loss is expressed as

$$\mathcal{L}_{tlc} = d_{uu}^{fr} + \beta_w \times d_{ll}^{fr}. \quad (18)$$

Considering both luminance and color, the traffic light appearance loss \mathcal{L}_{tla} is the sum of loss \mathcal{L}_{tll} and \mathcal{L}_{tlc} .

F. Dual Feedback Learning Strategy

Although the OAMix module and traffic light appearance loss are beneficial for feature learning of SOC, the boosting is limited due to the low and relatively fixed learning frequency. In contrast to fixed learning schedules, humans use feedback to enhance the systematicity of learning strategies for skill acquisition [13], [14]. Inspired by such a feedback-based learning scheme, we propose a dual feedback learning strategy to dynamically adjust the learning frequency of SOC samples based on the current learning state.

Let the SOC sample sets of domain A and domain B be defined as X_{soc}^A and X_{soc}^B , respectively. Then, we evaluate the learning status of the model for SOC by comparing the appearance consistency loss of SOC with the global reconstruction loss, which determines whether the learning of SOC samples requires enhancement. Taking domain A as an example, given the values of the appearance consistency loss (i.e., Eq. (10)) for SOC and the global reconstruction loss (i.e., $MIDF(\mathbf{1}, \tilde{x}_{ra}, x_{ra})$) at moment $t-1$, defined as $Z_{As}^{(t-1)}$ and $Z_{Ag}^{(t-1)}$, respectively, the image sampled at moment t according to the dual feedback learning strategy can be expressed as

$$x_{ra}^{(t)} \in \begin{cases} X_{soc}^A, & \text{if } Z_{As}^{(t-1)} > Z_{Ag}^{(t-1)}. \\ X^A, & \text{otherwise.} \end{cases} \quad (19)$$

When $Z_{As}^{(t-1)}$ is greater than $Z_{Ag}^{(t-1)}$, the appearance learning for SOC is below the mean, which indicates that the model needs to enhance the learning frequency for SOC samples. Conversely, the model does not require changes to the original learning plan. The sampling strategy for domain B is also similar to Eq. (19). By dynamically adjusting the learning strategy through the dual feedback of both domains, the model can not only allocate learning resources more rationally (e.g., reduce redundant learning of simple samples), but also learn the features of the SOC efficiently.

G. Objective Function

In summary, the overall objective function of the proposed FoalGAN can be expressed as

$$\mathcal{L}_{all} = \mathcal{L}_{base} + \mathcal{L}_{bc} + \mathcal{L}_{ac} + \mathcal{L}_{tla}. \quad (20)$$

IV. EXPERIMENTS

In this section, we first introduce the datasets and evaluation metrics for the NTIR2DC task. Subsequently, we explain the annotation of the Brno dataset and the implementation details of FoalGAN. Then, experimental results on the FLIR and Brno datasets are presented. Next, we perform an ablation analysis to verify the validity of the proposed modules, losses, and strategies. At last, some discussions of the experimental results are presented.

A. Datasets and Evaluation Metrics

1) *Datasets*: Due to the poor quality of the NTIR images in the KAIST [46] dataset (e.g., the SOC regions are too blurred to be detected), we choose the FLIR and Brno datasets to evaluate the translation performance of the SOC. The FLIR Thermal Starter Dataset [47] provides an annotated TIR image set and a non-annotated RGB image set for training and validating object detection models. Through the same data split as in [4], we finally obtain 5447 DC images and 2899 NTIR images for training, while an additional 490 NTIR images are used for testing.

The Brno Urban Dataset [15] records data from multiple sensors in the city of Brno for the study of autonomous driving tasks. The data were collected in sunny, cloudy and rainy environments. Three videos of sunny days in the DC domain, and two videos of cloudy days and one video of rainy days in the NTIR domain were selected as training data. An additional cloudy video and a rainy video in the NTIR domain were selected as test data. To eliminate redundant data at adjacent times, we re-sampled the videos at one frame per second, and finally obtained 2574 DC images and 2383 NTIR images for model training. Similarly, we re-sampled the tested NTIR videos at an interval of 60 frames, and finally selected 500 NTIR images randomly as the test set².

In order to remove the black areas on both sides in some images, according to [4], we first resize the training images to a resolution of 500×400 , and then the 360×288 resolution images obtained by center cropping are used as training data.

2) *Evaluation Metrics*: To evaluate the performance for image content preservation at each level, we conduct experiments on three vision tasks: semantic segmentation, object detection, and edge preservation.

Intersection-over-Union (IoU) [48] is a widely used metric in semantic segmentation tasks. The mean value of IoU for all classes, denoted as mIoU, is adopted to evaluate the semantic consistency of NTIR image colorization methods.

Average precision (AP) [49] denotes the average detection precision of the object detection model under different recalls. The mean value of AP for all categories, defined as mAP, is selected as an overall evaluation metric.

²See <https://github.com/FuyaLuo/FoalGAN/> for detailed sample selection.

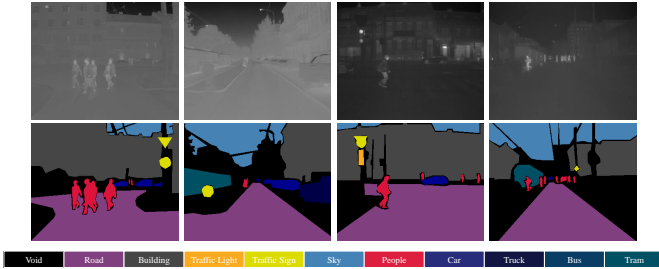


Fig. 5. Examples of NTIR images from the Brno dataset (top row) and our annotated segmentation masks (bottom row).

APCE [4] is the average precision of Canny edges under multi-threshold conditions, and is employed to evaluate the edge preservation performance of the NTIR2DC model.

B. Image Annotation of the Brno Dataset

To evaluate the semantic preservation performance of the NTIR2DC task, we selected and annotated a subset of Brno dataset with their pixel-level category labels. Considering the diversity of weather, 500 NTIR images in cloudy and rainy environments were selected for annotation. Due to the low contrast and ambiguous boundaries of NTIR images, as shown in Fig. 5, we define ten categories and use the LabelMe³ toolbox to annotate only their identified corresponding regions. The labeled categories are road, building, traffic light, traffic sign, sky, people, car, truck, bus, and tram.

C. Experimental Settings and Implementation Details

We compare FoalGAN with other NTIR2DC methods such as PearlGAN [4] and MornGAN [22], as well as some low-light enhancement methods (e.g., ToDayGAN [11]) and prevalent I2I translation methods (e.g., CycleGAN [8], UNIT [23] and DRIT++ [10]). We follow the instructions of these methods in order to establish a fair setting for comparison.

FoalGAN is implemented using PyTorch. We train the model using the Adam [50] optimizer with $(\beta_1, \beta_2) = (0.5, 0.999)$ on NVIDIA RTX 3090 GPUs. The batch size is set to 1 for all experiments. The learning rate of the whole training process is maintained at 0.0002. The total number of training epochs for the FLIR and Brno datasets are 100 and 160, respectively. In Eq. (1), the temperature threshold θ_{tem} is empirically set to 0.25 based on the brightness difference between categories in the NTIR images. Referring to the gradient threshold in SGA [4] loss, the similarity threshold θ_{sim} in Eq. (2) is set to 0.8. In Section III, the SOC set C_{so} includes three categories: traffic light, traffic sign, and motorcycle. For data augmentation, we flip the images horizontally with a probability of 0.5, and randomly crop them to the size of 256×256 . The number of parameters of our model is about 46.7 MB, and the inference speed on an NVIDIA RTX 3090 GPU is about 0.01 seconds for an input image with a resolution of 360×288 pixels.

Due to the lack of category annotation of NTIR images in the training set, we divided the training process into two

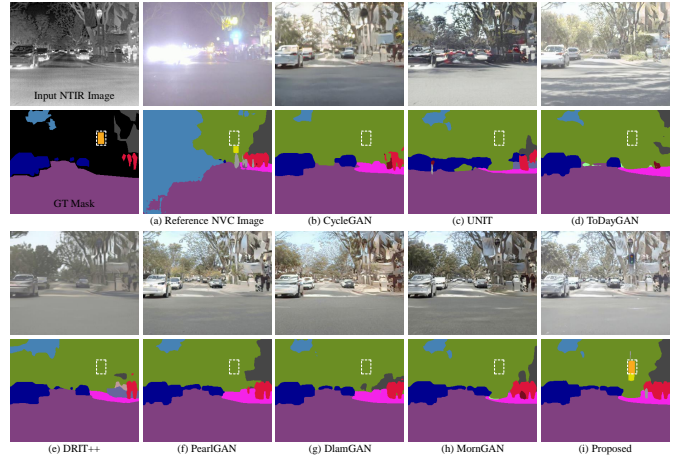


Fig. 6. The visual comparison of translation (the first row) and segmentation results (the second row) for different methods on the FLIR dataset. The areas in the white dotted boxes deserve attention.

phases: a pre-training phase and a feedback learning phase⁴. In the pre-training phase, the model introduces bias correction for learning based on MornGAN to determine the SOC sample sets X_{soc}^A and X_{soc}^B , and the training process is consistent with MornGAN [22]. In the feedback learning phase, the complete model dynamically adjusts the learning frequency of the SOC samples based on the current learning state, with a total number of iterations of approximately 110K.

Due to the lack of pixel-level annotations on the FLIR and Brno datasets, we evaluate the semantic segmentation performance of translated images using a scene parsing model HMSANet [43] trained on Cityscape [51], which considers both the feature plausibility and semantic consistency of colorization. Similarly, to measure the naturalness of object features, we utilize YOLOv7 [52], which is trained on the MS COCO [53] dataset as the evaluation model for object detection on the translated images.

D. Experiments on the FLIR Dataset

1) *Semantic Segmentation*: The translation results and corresponding segmentation outputs of various methods on the FLIR dataset are presented in Fig. 6. Column (a) represents the reference nighttime visible color (NVC) image and its semantic segmentation. Due to the blurring of features, the segmentation model HMSANet [43] is unable to identify traffic lights and cars in the glare region, which poses a great challenge to the visible-based scene perception system. All the compared I2I translation methods cannot generate plausible traffic lights, as shown in the white dashed box area. In contrast, the proposed model can recognize traffic lights in NTIR images and achieve reasonable colorization, which facilitates nighttime scene understanding. Moreover, directly below the white dashed box, all methods except ours fail to generate traffic signs recognized by the segmentation model, which demonstrates the superiority of FoalGAN in colorization of small objects.

³<https://github.com/CSAILVision/LabelMeAnnotationTool>.

⁴See <https://github.com/FuyaLuo/FoalGAN/> for implementation details.

TABLE I
SEMANTIC SEGMENTATION PERFORMANCE (IOU) ON THE TRANSLATED IMAGES BY DIFFERENT TRANSLATION METHODS ON THE FLIR DATASET.

	Road	Building	Sky	Person	Car	Truck	Bus	Traffic Light	Traffic Sign	Motorcycle	mIoU
Reference NVC image	95.2	53.7	1.0	40.3	56.6	2.5	70.1	9.4	5.2	0.0	33.4
CycleGAN [8]	97.2	19.6	89.4	67.1	79.3	0.3	0.8	1.5	0.0	0.0	35.5
UNIT [23]	96.3	48.3	92.5	59.5	63.7	0.6	49.4	5.9	0.0	12.4	42.9
ToDayGAN [11]	97.0	42.3	83.2	56.3	76.5	0.0	6.5	1.4	0.0	2.5	36.6
DRIT++ [10]	98.2	16.1	75.3	38.3	79.4	0.0	3.2	2.6	0.0	0.0	31.3
PearlGAN [4]	98.6	71.0	95.1	84.3	89.1	1.5	0.0	4.4	0.0	12.2	45.6
DlamGAN [5]	97.4	67.2	94.0	74.0	89.1	2.1	0.3	6.3	0.1	36.2	46.7
MornGAN [22]	98.7	84.0	96.8	94.5	95.6	1.2	22.8	22.0	0.7	40.4	55.7
Proposed	98.7	82.7	96.1	94.1	96.3	3.2	22.2	57.2	4.0	56.6	61.1



Fig. 7. Visual comparison of detection results on the FLIR dataset by YOLOv7 model [52]. The parts covered by red and green dashed boxes show the enlarged patches in the corresponding images. Colors in the detection results that do not intersect with GT represent undefined categories of the FLIR dataset as identified by the detector.

Table I reports a quantitative comparison of the semantic consistency performance on the FLIR dataset. The proposed method achieves comparable performance with MornGAN in semantic preservation of large sample categories (i.e., road, building, sky, pedestrian, and car). And all the compared methods have poor translation performance for small sample categories (i.e., truck, bus, traffic light, traffic sign, and motorcycle) due to few available samples and diverse colors. However, benefiting from the feedback-based appearance learning scheme, the proposed method significantly outperforms other methods in terms of semantic consistency on SOC (i.e., traffic light, traffic sign, and motorcycle). Overall, the proposed method leads other methods in terms of scene layout maintenance by a significant margin (i.e., at least 5.4%).

2) *Object Detection*: Fig. 7 shows the qualitative translation and detection result comparisons, wherein the second row is the zoomed-in image of the corresponding area. As shown in the dashed box, all compared approaches fail to generate plausible pedestrians. Moreover, CycleGAN, ToDayGAN and DRIT++ are unable to realistically translate cars. On the contrary, the proposed FoalGAN can not only achieve reasonable colorization for small-sized cars, but also maintain the complete pedestrian structure, which illustrates the superiority of the proposed method for small object preservation. In addition, more pedestrians are detected from our translated images than from the NVC images by the object detection model of YOLOv7 [52].

As the bounding-box annotation of the FLIR dataset covers only three categories (i.e., pedestrian, bicycle, and car),

TABLE II
OBJECT DETECTION PERFORMANCE (AP) ON THE TRANSLATED IMAGES BY DIFFERENT TRANSLATION METHODS ON THE FLIR DATASET, COMPUTED AT A SINGLE IOU OF 0.50.

	Person	Bicycle	Car	mAP
Reference NVC image	8.3	2.1	10.9	7.1
CycleGAN [8]	21.0	3.2	38.4	20.9
UNIT [23]	17.5	11.2	20.5	16.4
ToDayGAN [11]	25.7	1.9	53.6	27.1
DRIT++ [10]	20.6	2.1	48.5	23.8
PearlGAN [4]	59.3	25.1	75.4	53.3
DlamGAN [5]	53.4	18.6	72.3	48.1
MornGAN [22]	82.7	29.7	82.9	65.1
Proposed	84.6	34.7	85.6	68.3

quantitative comparison of various colorization results for object detection is shown in Table II. The proposed method consistently outperforms other methods in terms of object preservation for all classes. It is worth mentioning that for the retention of challenging bicycles, the proposed FoalGAN still outperforms the second-ranked MornGAN by 5%.

3) *Edge Preservation*: In Fig. 8, we qualitatively compare the ability of edge preservation of different I2I translation methods, and the second row shows the zoomed-in patches of the corresponding area fused with the edges of the original NTIR image. As shown in the blue dashed box, the edges in the DRIT++ results are outwardly expanded relative to the edges of traffic light in the NTIR image, while the edges of the other compared methods are inwardly shrunk. On the contrary, the edges of the proposed method are able to fit perfectly with the original edges, even though the intensity of edges on the left side of traffic light is extremely small. Similarly, as shown in the orange dashed box, all methods except ours fail to preserve the left edge of the traffic light, which illustrates the superiority of the proposed method in terms of structure preservation of small objects.

As the Canny edges in the Fig. 8 are only the results of a fixed threshold, we exploit the APCE metric, which covers multiple thresholds to comprehensively evaluate the edge consistency performance, as shown in Fig. 9 (a). We can find that the proposed method dramatically outperforms other methods in edge consistency at all thresholds and is far superior to the second ranked MornGAN by 11%.

E. Experiments on the Brno Dataset

Different from FLIR [47], Brno [15] is a more challenging dataset with NTIR images under multiple weather conditions.

TABLE III
SEMANTIC SEGMENTATION PERFORMANCE (IoU) ON THE TRANSLATED IMAGES BY DIFFERENT TRANSLATION METHODS ON THE BRNO DATASET.

	Road	Building	Sky	Person	Car	Bus	Tram	Traffic Light	Traffic Sign	mIoU
Reference NVC image	81.2	53.2	0.0	10.8	43.5	0.0	25.7	3.3	3.6	24.6
CycleGAN [8]	82.2	40.3	77.8	9.0	53.4	0.5	6.9	3.4	2.5	30.7
UNIT [23]	91.0	53.3	85.8	21.4	68.7	6.8	13.2	9.8	3.8	39.3
ToDayGAN [11]	93.9	48.7	67.5	29.4	65.0	6.9	17.5	7.3	1.6	37.5
DRIT++ [10]	93.4	55.1	74.0	19.4	68.6	0.6	12.9	2.4	2.9	36.6
PearlGAN [4]	82.1	52.4	92.3	44.0	50.5	5.1	8.5	25.8	3.8	40.5
DiamGAN [5]	82.2	58.0	91.9	44.7	58.0	11.6	9.6	37.2	2.8	44.0
MornGAN [22]	85.7	88.8	84.6	54.4	65.0	1.4	13.6	41.3	5.3	48.9
Proposed	92.6	90.4	86.5	59.3	72.1	6.4	37.0	68.8	28.0	60.1

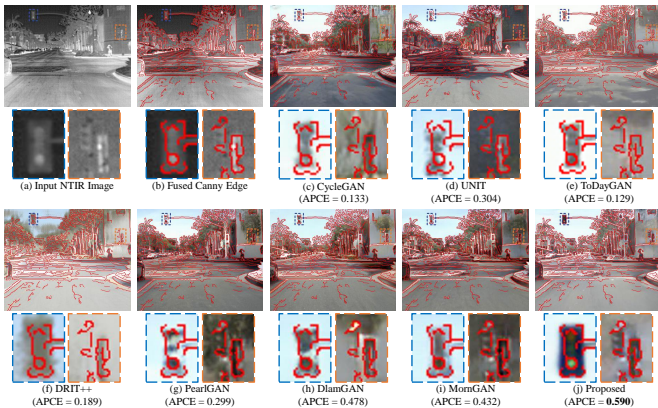


Fig. 8. Visual comparison of geometric consistency on the FLIR dataset. The second row shows the enlarged results of the corresponding regions after fusion with the edges. The edges in red are extracted by the Canny detector from the input NTIR image.

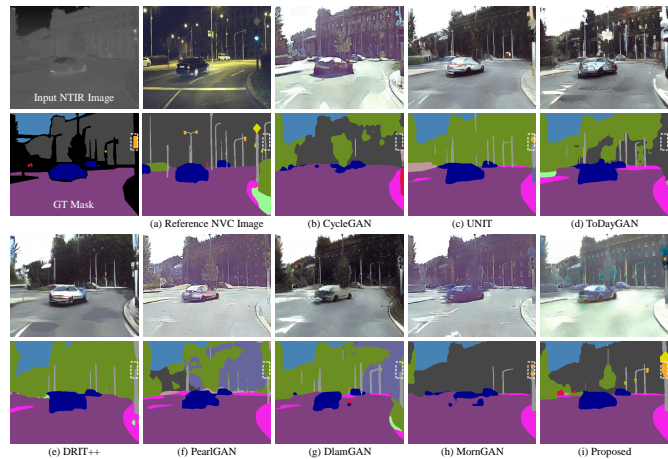


Fig. 10. The visual comparison of translation (the first row) and segmentation performance (the second row) of different methods on the Brno dataset. The areas in white dotted boxes deserve attention.

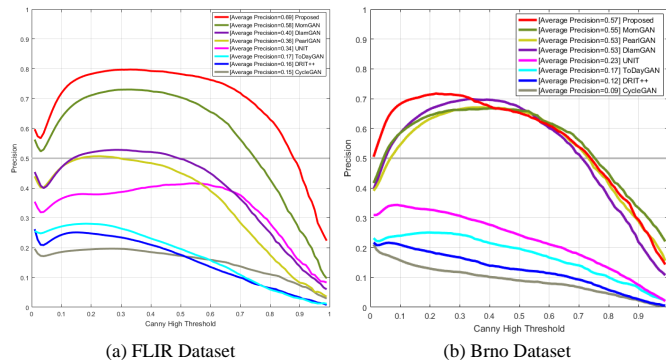


Fig. 9. APCE results of different translation methods on the FLIR and Brno datasets.

1) *Semantic Segmentation*: Fig. 10 presents the translated results and the segmentation outputs of various methods on the Brno dataset. As shown in the white dashed box, UNIT and MornGAN can generate some of the traffic light features, while none of the other comparison methods can generate plausible traffic lights. Unlike other methods, the proposed FoalGAN can retain the complete traffic light structure to facilitate the recognition of segmentation models. In addition, our translation images are more beneficial for the detection of pedestrians on the left side compared with the original NVC images.

Furthermore, a quantitative comparison of the semantic

preservation performance of various I2I translation methods is shown in Table III. The proposed approach achieves the best results in terms of semantic preservation for most categories except three (i.e., road, sky, and bus). Among them, FoalGAN has a remarkable advantage (i.e., at least 20%) over other methods in the translation of traffic lights and traffic signs, which illustrates the superiority of the proposed method for appearance learning of SOC. In general, FoalGAN has a substantial lead (i.e., at least 12.2%) in semantic consistency of colorization relative to other methods.

2) *Edge Preservation*: The qualitative comparison of edge preservation on the Brno dataset is shown in Fig. 11. As shown in the blue dashed box, compared with the edges of tree in the NTIR image, the results of UNIT are inwardly contracted, while the results of the other compared methods are outwardly expanded. Unlike previous methods, the colorization result of FoalGAN can fit closely to the edges of the original image. For very thin wires, as shown in the orange dashed box, all methods except ours are unable to maintain the structure of the horizontal wire.

Further, the edge consistency comparison under the multi-threshold condition is shown in Fig. 9 (b). Considering all the thresholds, the proposed method still exhibits high performance in the edge consistency of the translation.

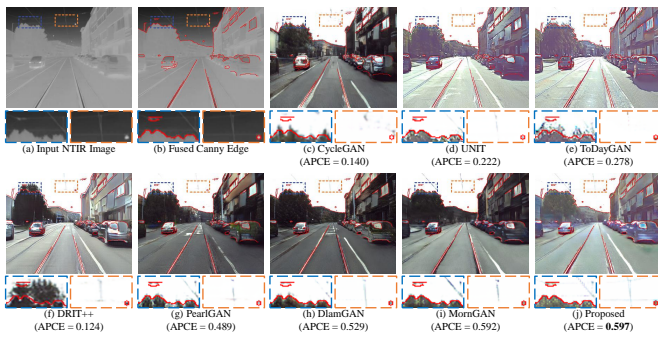


Fig. 11. Visual comparison of geometric consistency on the Brno dataset. The second row shows the enlarged results of the corresponding regions after fusion with the edges. The edges in red are extracted by the Canny detector from the input NTIR image.

TABLE IV

QUANTITATIVE ABLATION STUDY ON THE FLIR DATASET. “BC” MEANS THE BIAS CORRECTION LOSS AND CORRESPONDING PROCESS. “OAMIX+” MEANS THE OCCLUSION-AWARE MIXUP MODULE AND CORRESPONDING APPEARANCE CONSISTENCY LOSS. “TLLL” MEANS THE TRAFFIC LIGHT LUMINANCE LOSS. “TLCL” MEANS THE TRAFFIC LIGHT COLOR LOSS. “DFLS” MEANS THE DUAL FEEDBACK LEARNING STRATEGY. “MIOU.A” AND “MIOU.S” DENOTE THE MIOU RESULTS FOR THE SET OF ALL CATEGORIES AND SMALL OBJECT CATEGORIES, RESPECTIVELY.

Baseline	BC	OAMix+	TLLL	TLCL	DFLS	mIoU.A(%)	mIoU.S(%)	APCE
✓						55.7	21.0	0.58
✓	✓					56.0	22.1	0.57
✓	✓	✓				57.8	26.9	0.65
✓	✓	✓	✓			58.1	27.6	0.65
✓	✓	✓	✓	✓		58.7	30.0	0.69
✓	✓	✓	✓	✓	✓	61.1	39.3	0.69

F. Ablation Study

Ablation analysis is performed on the FLIR dataset to discuss the validity of each component of FoalGAN. The results of the ablation analysis are shown in Table IV, and an example of a qualitative comparison is shown in Fig. 12. We can find that the baseline model has poor colorization performance for traffic lights (i.e., the high temperature region is colored black), which misleads the segmentation model to identify the region as building, as shown in the second column of the figure. Then, due to its focus on the fake NTIR image branch, the bias correction is limited for the performance improvement of colorization. Moreover, as shown in Table IV, the edge consistency decreases slightly due to the noise in the pseudo-labels. However, such a bias-correction process can reduce the mismatching of the fake NTIR image branch, which paves the way for subsequent reduction of the context dependence of object translation.

With the introduction of the OAMix module and the appearance consistency loss, as shown in Table IV, the semantic consistency of SOC is significantly improved and a large gain in the edge consistency is achieved. And the high temperature region in the NTIR image is partially mapped as red, as shown in the fourth column of Fig. 12. However, the lamp housing of the traffic light remains gray, which deviates from the real color distribution.

Further, as shown in the fifth column of Fig. 12, the traffic light luminance loss can make the light housing color more

plausible and the luminance distribution more reasonable. However, the color of the light in that position does not match the actual design. In the next experiment, traffic light color loss can reduce this color bias, i.e., by changing most of the yellow areas to green, as shown in the sixth column of Fig. 12. Moreover, the semantic preservation of SOC gets further enhancement, as shown in Table IV.

Ultimately, as shown in the last column of Fig. 12, the proposed dual feedback learning strategy not only benefits the appearance learning of traffic lights, but also significantly reduces the content distortion during translation. In addition, we can find from Table IV a massive improvement in semantic consistency of SOC, which demonstrates the effectiveness of the proposed strategy.

G. Discussion

In this section, we analyze (1) the generalization capability of the proposed method, (2) the color accuracy of translated traffic lights, and (3) the limitations of FoalGAN.

TABLE V

RESULTS OF GENERALIZATION EXPERIMENTS. “AVE.” MEANS AVERAGE VALUE.

	mIoU(%)			APCE		
	B→F	F→B	AVE.	B→F	F→B	AVE.
CycleGAN [8]	14.3	19.3	16.8	0.06	0.07	0.07
UNIT [23]	34.5	20.8	27.7	0.25	0.16	0.21
ToDayGAN [11]	28.5	21.3	24.9	0.17	0.15	0.16
DRIT++ [10]	25.9	28.3	27.1	0.15	0.20	0.18
PearlGAN [4]	45.0	40.7	42.9	0.42	0.48	0.45
DlamGAN [5]	41.1	43.6	42.4	0.48	0.54	0.51
MornGAN [22]	47.1	56.0	51.6	0.43	0.63	0.53
Proposed	51.9	56.1	54.0	0.57	0.63	0.60

1) *Generalization Experiments*: In order to explore the generalization ability of various I2I translation methods to out-of-domain distributions, we apply each model trained on the Brno dataset to the FLIR dataset abbreviated as B→F and vice versa as F→B. The results are shown in Table V. For the performance of semantic preservation, we can find that the proposed method obtains the best mIoU among all methods for both B→F and F→B experiments. Similarly, for the comparison of edge consistency during translation, FoalGAN consistently keeps high performance for APCE in both experimental modes. In summary, the results demonstrate the stronger generalization capability of the proposed method for domain shift.

TABLE VI

COMPARISON OF THE NUMBER OF INSTANCES WITH CORRECT COLOR IN THE TRANSLATED TRAFFIC LIGHTS.

	All Compared Methods	Proposed	Total Instances
FLIR Dataset	0	60	457
Brno Dataset	0	17	144

2) *Color Accuracy of Translated Traffic Lights*: Since the color of signal is important for the decision making of driving systems, we count the color accuracy of traffic lights in the translation results. The results are shown in Table VI, where all compared I2I translation methods consistently fail to generate

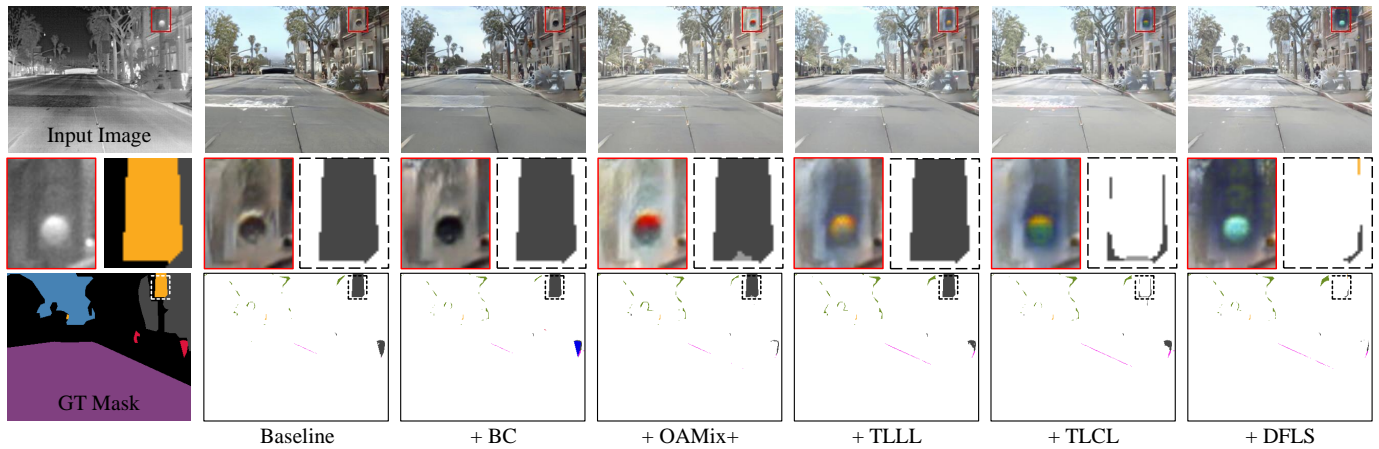


Fig. 12. Visual results of ablation study on the FLIR dataset. The first row shows the input NTIR image and the translated images by different versions of our model. In the second row, the parts covered by red boxes show the enlarged cropped regions in the corresponding image. The black dotted box is the result of zooming in on the corresponding area in the third row. The third row shows the error maps of the semantic segmentation results, where the white areas indicate the correct regions or unlabeled regions. The meanings of BC, OAMix+, TLLL, TLCL, and DFSL can be found in Table IV.



Fig. 13. Visual comparison of the colors of traffic light instances in the translation results.

any traffic light instances with correct color, while FoalGAN can achieve some color accuracy on both datasets. Due to the tiny temperature difference between red and green lights in most NTIR images, as shown in Fig. 13, it is extremely challenging to achieve correct traffic light colorization in the NTIR2DC task. Compared with the poor performance of other methods for traffic light colorization, the proposed method can generate plausible traffic lights and correctly infer the colors of some signals.

3) *Limitations*: Fig. 14 shows four failure cases of FoalGAN, where the input images in the first two columns are from the FLIR dataset, and the remaining images are from the Brno dataset. As shown in the first and third columns, the pedestrian’s faces are unrealistic due to the diversity of perspectives and scales. A potential solution to this problem is to design new loss functions to encourage the alignment of facial features from different perspectives with the real features. In addition, the colorization for large objects is poor due to the lack of modeling for long-range dependencies, as shown in the second and fourth columns. To solve this problem, more attempts should be made to design corresponding modules to recognize large objects, and to introduce new losses to encourage the continuity of feature distribution in space.

V. CONCLUSION

In this paper, we developed a new learning framework called FoalGAN to achieve colorization of NTIR images.



Fig. 14. Visualization of four failure cases. The first and second rows show the NTIR images and their translation results, respectively.

Benefiting from the proposed dual feedback learning strategy, the framework enabled the great improvement of the translation performance of small object categories. An OAMix module and the corresponding appearance consistency loss were proposed to reduce the context dependence of object translation. In addition, a traffic light appearance loss was designed to enhance the realism of traffic light. Moreover, we annotated a subset of the Brno dataset with pixel-wise category labels to further catalyze research on colorization and semantic segmentation of NTIR images. Comprehensive experiments demonstrate the superiority of FoalGAN for semantic preservation and edge consistency in the NTIR2DC task. In the future, designing a more generalized NTIR2DC model that can be applied to a wide range of weather and various imaging devices is a promising research direction.

ACKNOWLEDGMENTS

This work was supported by Aviation Equipment Bureau of Naval Equipment Department (21AZ0501), Sichuan Science and Technology Program (2022ZYD0112) and National Natural Science Foundation of China (62076055).

REFERENCES

- [1] C. Li, C. Zhu, J. Zhang, B. Luo, X. Wu, and J. Tang, “Learning local-global multi-graph descriptors for rgb-t object tracking,” *IEEE Trans. Circuits Syst. Video Technol.*, vol. 29, no. 10, pp. 2913–2926, 2018.

- [2] C. Li, X. Wang, L. Zhang, J. Tang, H. Wu, and L. Lin, "Weighted low-rank decomposition for robust grayscale-thermal foreground detection," *IEEE Trans. Circuits Syst. Video Technol.*, vol. 27, no. 4, pp. 725–738, 2016.
- [3] G. W. Stuart and P. K. Hughes, "Towards an understanding of the effect of night vision display imagery on scene recognition," *The Ergonomics Open Journal*, vol. 2, no. 1, 2009.
- [4] F. Luo, Y. Li, G. Zeng, P. Peng, G. Wang, and Y. Li, "Thermal infrared image colorization for nighttime driving scenes with top-down guided attention," *IEEE Trans. Intell. Transp. Syst.*, vol. 23, no. 9, pp. 15 808–15 823, 2022.
- [5] F. Luo, Y. Cao, and Y. Li, "Nighttime thermal infrared image colorization with dynamic label mining," in *International Conference on Image and Graphics*. Springer, 2021, pp. 388–399.
- [6] P. Isola, J.-Y. Zhu, T. Zhou, and A. A. Efros, "Image-to-image translation with conditional adversarial networks," in *Proc. CVPR*, 2017, pp. 1125–1134.
- [7] I. J. Goodfellow, J. Pouget-Abadie, M. Mirza, B. Xu, D. Warde-Farley, S. Ozair, A. C. Courville, and Y. Bengio, "Generative adversarial nets," in *Proc. NeurIPS*, 2014.
- [8] J.-Y. Zhu, T. Park, P. Isola, and A. A. Efros, "Unpaired image-to-image translation using cycle-consistent adversarial networks," in *Proc. ICCV*, 2017, pp. 2223–2232.
- [9] X. Huang, M.-Y. Liu, S. Belongie, and J. Kautz, "Multimodal unsupervised image-to-image translation," in *Proc. ECCV*, 2018, pp. 172–189.
- [10] H.-Y. Lee, H.-Y. Tseng, Q. Mao, J.-B. Huang, Y.-D. Lu, M. Singh, and M.-H. Yang, "Drit++: Diverse image-to-image translation via disentangled representations," *International Journal of Computer Vision*, vol. 128, no. 10, pp. 2402–2417, 2020.
- [11] A. Anoshkeh, T. Sattler, R. Timofte, M. Pollefeys, and L. Van Gool, "Night-to-day image translation for retrieval-based localization," in *ICRA*, 2019, pp. 5958–5964.
- [12] H. Zhang, M. Cisse, Y. N. Dauphin, and D. Lopez-Paz, "mixup: Beyond empirical risk minimization," in *Proc. ICLR*, 2018.
- [13] R. Vollmeyer and F. Rheinberg, "A surprising effect of feedback on learning," *Learning and instruction*, vol. 15, no. 6, pp. 589–602, 2005.
- [14] C. D. B. Luft, "Learning from feedback: The neural mechanisms of feedback processing facilitating better performance," *Behavioural brain research*, vol. 261, pp. 356–368, 2014.
- [15] A. Ligocki, A. Jelinek, and L. Zalud, "Brno urban dataset-the new data for self-driving agents and mapping tasks," in *Proc. ICRA*. IEEE, 2020, pp. 3284–3290.
- [16] A. Berg, J. Ahlberg, and M. Felsberg, "Generating visible spectrum images from thermal infrared," in *Proc. CVPR Workshops*, 2018, pp. 1143–1152.
- [17] N. Bhat, N. Saggua, S. Kumar *et al.*, "Generating visible spectrum images from thermal infrared using conditional generative adversarial networks," in *JCCES*, 2020, pp. 1390–1394.
- [18] X. Kuang, J. Zhu, X. Sui, Y. Liu, C. Liu, Q. Chen, and G. Gu, "Thermal infrared colorization via conditional generative adversarial network," *Infrared Physics & Technology*, p. 103338, 2020.
- [19] T. Le-Tien, T. H. D. Quang, H. Y. Vy, T. Nguyen-Thanh, and H. Phan-Xuan, "Gan-based thermal infrared image colorization for enhancing object identification," in *Proc. ISEE*. IEEE, 2021, pp. 90–94.
- [20] Y. Zhao, L.-M. Po, K.-W. Cheung, W.-Y. Yu, and Y. A. U. Rehman, "Scgan: saliency map-guided colorization with generative adversarial network," *IEEE Trans. Circuits Syst. Video Technol.*, vol. 31, no. 8, pp. 3062–3077, 2020.
- [21] A. Nyberg, A. Eldesokey, D. Bergstrom, and D. Gustafsson, "Unpaired thermal to visible spectrum transfer using adversarial training," in *Proc. ECCV*, 2018, pp. 0–0.
- [22] F.-Y. Luo, Y.-J. Cao, K.-F. Yang, and Y.-J. Li, "Memory-guided collaborative attention for nighttime thermal infrared image colorization," *arXiv preprint arXiv:2208.02960*, 2022.
- [23] M.-Y. Liu, T. Breuel, and J. Kautz, "Unsupervised image-to-image translation networks," in *Proc. NeurIPS*, 2017.
- [24] Z. Zheng, Y. Wu, X. Han, and J. Shi, "Forkgan: Seeing into the rainy night," in *Proc. ECCV*. Springer, 2020, pp. 155–170.
- [25] D. Bhattacharjee, S. Kim, G. Vizier, and M. Salzmann, "Dunit: Detection-based unsupervised image-to-image translation," in *Proc. CVPR*, 2020, pp. 4787–4796.
- [26] L. Fu, H. Yu, F. Juefei-Xu, J. Li, Q. Guo, and S. Wang, "Let there be light: Improved traffic surveillance via detail preserving night-to-day transfer," *IEEE Trans. Circuits Syst. Video Technol.*, 2021.
- [27] S.-W. Huang, C.-T. Lin, S.-P. Chen, Y.-Y. Wu, P.-H. Hsu, and S.-H. Lai, "Auggan: Cross domain adaptation with gan-based data augmentation," in *Proc. ECCV*, 2018, pp. 718–731.
- [28] A. Cherian and A. Sullivan, "Sem-gan: semantically-consistent image-to-image translation," in *Proc. WACV*. IEEE, 2019, pp. 1797–1806.
- [29] D. S. Tan, Y.-X. Lin, and K.-L. Hua, "Incremental learning of multi-domain image-to-image translations," *IEEE Trans. Circuits Syst. Video Technol.*, vol. 31, no. 4, pp. 1526–1539, 2020.
- [30] A. Ford and F. A. Ford, *Modeling the environment: an introduction to system dynamics models of environmental systems*. Island press, 1999.
- [31] J. Hupé, A. James, B. Payne, S. Lomber, P. Girard, and J. Bullier, "Cortical feedback improves discrimination between figure and background by v1, v2 and v3 neurons," *Nature*, vol. 394, no. 6695, pp. 784–787, 1998.
- [32] C. D. Gilbert and M. Sigman, "Brain states: top-down influences in sensory processing," *Neuron*, vol. 54, no. 5, pp. 677–696, 2007.
- [33] D. Wyatte, T. Curran, and R. O'Reilly, "The limits of feedforward vision: Recurrent processing promotes robust object recognition when objects are degraded," *Journal of Cognitive Neuroscience*, vol. 24, no. 11, pp. 2248–2261, 2012.
- [34] M. F. Stollenga, J. Masci, F. Gomez, and J. Schmidhuber, "Deep networks with internal selective attention through feedback connections," *Proc. NeurIPS*, vol. 27, 2014.
- [35] A. R. Zamir, T.-L. Wu, L. Sun, W. B. Shen, B. E. Shi, J. Malik, and S. Savarese, "Feedback networks," in *Proc. CVPR*, 2017, pp. 1308–1317.
- [36] Z. Li, J. Yang, Z. Liu, X. Yang, G. Jeon, and W. Wu, "Feedback network for image super-resolution," in *Proc. CVPR*, 2019, pp. 3867–3876.
- [37] X. Song, D. Zhou, W. Li, H. Ding, Y. Dai, and L. Zhang, "Wsamf-net: Wavelet spatial attention based multi-stream feedback network for single image dehazing," *IEEE Trans. Circuits Syst. Video Technol.*, 2022.
- [38] S. Yun, D. Han, S. J. Oh, S. Chun, J. Choe, and Y. Yoo, "Cutmix: Regularization strategy to train strong classifiers with localizable features," in *Proc. ICCV*, 2019, pp. 6023–6032.
- [39] V. Olsson, W. Tranheden, J. Pinto, and L. Svensson, "Classmix: Segmentation-based data augmentation for semi-supervised learning," in *Proc. WACV*, 2021, pp. 1369–1378.
- [40] Q. Zhou, Z. Feng, Q. Gu, J. Pang, G. Cheng, X. Lu, J. Shi, and L. Ma, "Context-aware mixup for domain adaptive semantic segmentation," *IEEE Trans. Circuits Syst. Video Technol.*, 2022.
- [41] R. Takahashi, T. Matsubara, and K. Uehara, "Data augmentation using random image cropping and patching for deep cnns," *IEEE Trans. Circuits Syst. Video Technol.*, vol. 30, no. 9, pp. 2917–2931, 2019.
- [42] Y. Wu, A. Kirillov, F. Massa, W.-Y. Lo, and R. Girshick, "Detectron2," <https://github.com/facebookresearch/detectron2>, 2019.
- [43] A. Tao, K. Sapra, and B. Catanzaro, "Hierarchical multi-scale attention for semantic segmentation," *arXiv preprint arXiv:2005.10821*, 2020.
- [44] G. Neuhold, T. Ollmann, S. Rota Bulo, and P. Kontschieder, "The mapillary vistas dataset for semantic understanding of street scenes," in *Proc. ICCV*, 2017, pp. 4990–4999.
- [45] Z. Wang, A. C. Bovik, H. R. Sheikh, and E. P. Simoncelli, "Image quality assessment: from error visibility to structural similarity," *IEEE Trans. Image Process.*, vol. 13, no. 4, pp. 600–612, 2004.
- [46] S. Hwang, J. Park, N. Kim, Y. Choi, and I. So Kweon, "Multispectral pedestrian detection: Benchmark dataset and baseline," in *Proc. CVPR*, 2015, pp. 1037–1045.
- [47] F.A.Group, "Flir thermal dataset for algorithm training," <https://www.flir.co.uk/oem/adas/adas-dataset-form/>, May 2019.
- [48] M. Everingham, S. A. Eslami, L. Van Gool, C. K. Williams, J. Winn, and A. Zisserman, "The pascal visual object classes challenge: A retrospective," *International journal of computer vision*, vol. 111, no. 1, pp. 98–136, 2015.
- [49] M. Everingham, L. Van Gool, C. K. Williams, J. Winn, and A. Zisserman, "The pascal visual object classes (voc) challenge," *International journal of computer vision*, vol. 88, no. 2, pp. 303–338, 2010.
- [50] D. P. Kingma and J. Ba, "Adam: A method for stochastic optimization," in *ICLR (Poster)*, 2015.
- [51] M. Cordts, M. Omran, S. Ramos, T. Rehfeld, M. Enzweiler, R. Benenson, U. Franke, S. Roth, and B. Schiele, "The cityscapes dataset for semantic urban scene understanding," in *Proc. CVPR*, 2016, pp. 3213–3223.
- [52] C.-Y. Wang, A. Bochkovskiy, and H.-Y. M. Liao, "Yolov7: Trainable bag-of-freebies sets new state-of-the-art for real-time object detectors," *arXiv preprint arXiv:2207.02696*, 2022.
- [53] T.-Y. Lin, M. Maire, S. Belongie, J. Hays, P. Perona, D. Ramanan, P. Dollár, and C. L. Zitnick, "Microsoft coco: Common objects in context," in *Proc. ECCV*, 2014, pp. 740–755.